Intraseasonal Modulation of the North Pacific Storm Track by Tropical Convection in Boreal Winter

YI DENG AND TIANYU JIANG

School of Earth and Atmospheric Sciences, Georgia Institute of Technology, Atlanta, Georgia

(Manuscript received 12 February 2010, in final form 12 October 2010)

ABSTRACT

The modulation of the North Pacific storm track by tropical convection on intraseasonal time scales (30–90 days) in boreal winter (December–March) is investigated using the NCEP–NCAR reanalysis and NOAA satellite outgoing longwave radiation (OLR) data. Multivariate empirical orthogonal function (MEOF) analysis and case compositing based upon the principal components (PCs) of the EOFs reveal substantial changes in the structure and intensity of the Pacific storm track quantified by vertically (925–200 mb) averaged synoptic eddy kinetic energy (SEKE) during the course of a typical Madden–Julian oscillation (MJO) event. The storm-track response is characterized by an amplitude-varying dipole propagating northeastward as the center of the anomalous tropical convection moves eastward across the eastern Indian Ocean and the western-central Pacific. A diagnosis of the SEKE budget indicates that the storm-track anomaly is induced primarily by changes in the convergence of energy flux, baroclinic conversion, and energy generation due to the interaction between synoptic eddies and intraseasonal flow anomalies. This demonstrates the important roles played by eddy–mean flow interaction and eddy–eddy interaction in the development of the extratropical response to MJO variability. The feedback of synoptic eddy to intraseasonal flow anomalies is pronounced: when the center of the enhanced tropical convection is located over the Maritime Continent (western Pacific), the anomalous synoptic eddy forcing partly drives an upper-tropospheric anticyclonic (cyclonic) and, to its south, a cyclonic (anticyclonic) circulation anomaly over the North Pacific. Associated with the storm-track anomaly, a three-band (dry–wet–dry) anomaly in both precipitable water and surface precipitation propagates poleward over the eastern North Pacific and induces intraseasonal variations in the winter hydroclimate over western North America.

1. Introduction

Storm tracks are extratropical regions characterized by strong activity of synoptic-scale disturbances (Blackmon 1976). Cyclones and anticyclones comprising a storm track are responsible for most of the severe and hazardous weather in winter, such as ice storms, blizzards, and cold-air outbreaks (Rauber et al. 2008). Storm tracks also play a key role in the global climate system due to the efficient transport of heat, momentum, and moisture by synoptic eddies in the extratropical troposphere in winter (e.g., Blackmon et al. 1977; Holopainen 1990). Considerable efforts have been made in the past three decades to investigate the dynamical processes leading to and maintaining a storm track; and in particular, to identify, understand, and simulate the variations of storm tracks on various time scales (for an excellent review of storm-track dynamics, see Chang et al. 2002). In the Northern Hemisphere (NH) cool season (October–March), the two major storm tracks—that is, the North Pacific and the North Atlantic storm tracks—exhibit distinctly different subseasonal evolutions. The Pacific storm track tends to attain its maximum intensity in late fall and early spring, while the intensity of the Atlantic storm track normally peaks in midwinter (January–February), in phase with the seasonal cycle of the local baroclinicity of the background flow (e.g., Nakamura 1992; Chang 2003). The cause of the so-called midwinter suppression of the Pacific storm track has been extensively studied. Processes that have been suggested to contribute to this suppression include the following: 1) trapping of baroclinic waves near the surface due to the steering level drop (Nakamura 1992); 2) the dissipative effect of diabatic heating, particularly condensational heating in the eddy potential energy budget (Chang 2001); 3) enhanced

Corresponding author address: Yi Deng, School of Earth and Atmospheric Sciences, Georgia Institute of Technology, 311 Ferst Dr., Atlanta, GA 30332-0340.
E-mail: yi.deng@eas.gatech.edu

DOI: 10.1175/2010JCLI3676.1

barotropic damping as a result of strengthened background flow deformation (Deng and Mak 2005, 2006); and 4) suppressed seeding disturbances upstream of the storm track (Penny et al. 2010). On interannual time scales, the variability of the Pacific storm track is related to the El Niño–Southern Oscillation (ENSO) with the storm track shifting equatorward (poleward) and eastward (westward) in an El Niño (La Niña) winter (Trenberth and Hurrell 1994; Straus and Shukla 1997). On decadal time scales, the two NH storm tracks have intensified during the second-half of the twentieth century, although the exact magnitude of the secular trends differs according to the estimates based upon the reanalysis data, radiosonde, and ship observations (Nakamura et al. 2002; Chang and Fu 2002; Chang 2007). The interdecadal variation of the Pacific storm track is modulated by the Pacific decadal oscillation (PDO) and inversely linked to the strength of the East Asian winter monsoon (Chang and Fu 2002; Nakamura et al. 2002). As a result of this variability, the ''midwinter suppression'' turned from being very pronounced in the early to mid-1980s to almost nonexistent in the following decade (Nakamura et al. 2002).

The interaction between synoptic eddies and a corresponding ''mean'' flow (or in a more generalized term, cross-frequency coupling) often proves to be critical in producing and maintaining the mean flow and storm-track anomalies. Through composite and empirical orthogonal function (EOF) analysis, Lau (1988) showed that variations in the winter monthly storm-track field are closely coupled to prominent atmospheric low-frequency modes (also known as teleconnections, Wallace and Gutzler 1981). For example, changes in the intensity of the Pacific storm track are often accompanied by a dipole structure in the upper-tropospheric geopotential height over the western Pacific (WP), resembling the WP pattern (e.g., Wallace and Gutzler 1981), while the meridional displacement of the storm track seems to be associated with the Pacific–North American (PNA) pattern. With a dissipative atmospheric model driven by a zonally symmetric forcing, Cai and Mak (1990) demonstrated that there exists a symbiotic relationship between the synoptic-scale and the low-frequency planetary-scale waves. The synoptic waves supply part of the energy they extract from the instantaneous zonal flow to the planetary waves through upscale energy cascade process, while the planetary waves create regions with strong baroclinicity where synoptic waves preferentially intensify. The significance of eddy–mean flow interaction and cross-frequency coupling is also widely recognized in studies that explore the dynamical nature of ''blocking'' or ''persistent anomalies'' (e.g., Dole and Gordon 1983; Trenberth 1986; Dole and Black 1990; Black 1997) and in studies that attempt to understand the phase transition of the annular modes (e.g., Rivière and Orlanski 2007; Gerber and Vallis 2009).

It is well known that transient eddies constitute a key component in the tropical–extratropical interaction. On one hand, fluctuations in the tropical sea surface temperature (SST) as a source of extratropical variability have been extensively studied owing to the prominence of the ENSO signal (e.g., Horel and Wallace 1981; Mo and Livezey 1986; Straus and Shukla 2002). The synoptic eddy forcing, in particular, the transient vorticity forcing associated with the storm-track anomalies, plays an essential role in setting up the extratropical response to ENSO because the direct stationary wave response to ENSO in the extratropics is relatively weak (Held et al. 1989; Hoerling and Ting 1994). On the other hand, midlatitude baroclinic waves can also drive tropical atmospheric motions, as discussed in early studies such as Mak (1969), Yanai and Lu (1983), and Zhang and Webster (1992). Diagnostic work by Kiladis and Weickmann (1992a,b) showed that the intraseasonal variation in the tropical convection over the eastern Pacific is typically associated with the intrusion of troughs from the midlatitudes. Kiladis (1998) further pointed out that Rossby wave activity propagating into the tropical eastern Pacific with midlatitude origins can modulate cloudiness, static stability, and vertical motion in the vicinity of the intertropical convergence zone (ITCZ), contribute to the variability of the ITCZ convection, and excite equatorially trapped Rossby modes. The propagation characteristics of these midlatitude waves depend on the properties of the background flow and can be interpreted using the ray-tracing theory formulated by Hoskins and Ambrizzi (1993). In particular, a ''critical latitude'' where the zonal phase velocity of the wave approaches the zonal velocity of the background flow acts as a barrier for Rossby wave propagation. This implies that stationary Rossby waves can only propagate into regions with background westerlies. Over the equator, upper-tropospheric westerlies (also known as the westerly duct) exist in winter over the eastern Pacific and the Atlantic, which allows cross-equatorial wave propagation (Tomas and Webster 1994). On interannual time scales, ENSO strongly modulates the location and strength of the westerly ''duct,'' hence the effectiveness of extratropical forcing on tropical variability. For example, in the El Niño winter of 1982/83, the westerlies moved eastward and the wave activity propagating into the central Pacific was largely suppressed (Kiladis 1998).

In addition to the classic view of the equatorward propagation of extratropical waves, Hoskins and Yang (2000) showed that high-latitude forcing of the tropics can also take the form of a direct projection onto the equatorial waves. This mechanism is potentially important

in organizing large-scale, deep tropical convection and initiating the most-pronounced tropical intraseasonal mode—the Madden–Julian oscillation (MJO; e.g., Madden and Julian 1972, 1994), whose origin was also suggested to be linked to instability of subtropical jets because of the strong coherence found between the tropical and subtropical planetary-scale waves (e.g., Straus and Lindzen 2000). Lin et al. (2009) identified over the North Atlantic a southward propagation and eastward expansion of upper-tropospheric zonal wind anomalies that are induced by the North Atlantic Oscillation (NAO), suggesting the potential role of extratropical low-frequency variability in leading to an MJO development.

The response of the extratropical circulation to the MJO in boreal winter has been actively studied in the past 30 years. Early work represented by Weickmann (1983) and Weickmann et al. (1985) demonstrated that the extratropical flow anomaly associated with the MJO variability is characterized by an eastward-propagating wavenumber-1 structure manifesting itself as an eccentric circumpolar vortex expanding (contracting) in regions of enhanced (suppressed) tropical convection. Weickmann et al. (1992, 1997) further investigated the atmospheric angular-momentum (AAM) cycle associated with the MJO and discussed the dynamics of the intraseasonal AAM oscillations. Most recently, Egger and Weickmann (2007) showed that during the life cycle of MJO, AAM anomalies of one sign first develop in the tropical upper troposphere and propagate downward and poleward to the subtropics in about two weeks, at which time AAM anomalies of the opposite sign start to appear in the tropical upper troposphere. Matthews et al. (2004) provided a good review on this topic but focused their discussion on the direct response to tropical heating that can be relatively well understood with a barotropic model—that is, quasi-stationary extratropical waves driven by a time-dependent tropical heat source derived from the observed MJO anomalies (e.g., Zhang and Hagos 2009). Pan and Li (2008) further suggested that synoptic-scale transients play a key role in the interaction between tropical intraseasonal oscillation and midlatitude low-frequency flow.

It is important to note that synoptic-scale transients (eddies) coming out of a storm track are nonstationary, and their influences on the tropics are not strictly constrained by the presence of an easterly ''barrier'' or a westerly duct (Yang and Hoskins 1996). In addition, given the observed storm-track variability across multiple time scales and the interaction between synoptic eddies and a large number of extratropical low-frequency modes, understanding the coupling between storm tracks and tropical intraseasonal oscillation becomes crucial to establish a complete picture of the global impact of the MJO. Matthews and Kiladis (1999) presented a pioneering analysis on the interaction between high-frequency transients and the MJO. They showed that during the early phase of the MJO when the enhanced convection is located over the east Indian Ocean, the upper-level Asian–Pacific jet and the tropical easterlies move westward, leading to a ''leakier'' waveguide along the jet and strengthened equatorward propagation of transient eddy activity into the tropical central Pacific. The enhanced convective variability associated with stronger transient eddy activity at the ITCZ projects back onto the intraseasonal time scale and becomes an integral part of the slowly evolving MJO signal. As the enhanced convection moves over the South Pacific convergence zone (SPCZ), a stronger Asian–Pacific jet (waveguide) extends over the central Pacific suppressing equatorward propagation of wave activity. Note that in this work, ''high frequency'' is obtained through a 6–25-day bandpass filter and does not correspond exactly to the typical 2–8-day time scale of synoptic eddies comprising a storm track—although the authors did mention that the magnitude of the anomalies of the perturbation kinetic energy almost doubled over the North Pacific when a 25-day high-pass filter was used in calculation. Therefore, there is still missing in the literature a comprehensive analysis of the intraseasonal modulation of the North Pacific storm track by tropical convection in boreal winter.

Practical implications of a tropical convection–induced storm-track anomaly include its projection onto regional hydroclimate variability. Myoung and Deng (2009) showed that by affecting coastal cyclonic activity, synoptic eddies existing in the Pacific storm track determine a large portion of the interannual variance of the winter precipitation characteristics in the western United States. Earlier studies, most notably Higgins and Mo (1997), Mo and Higgins (1998a), Mo (1999), and Higgins et al. (2000), demonstrated that tropical convection plays a vital role in setting up persistent North Pacific circulation anomalies, affecting strength of moisture transport and inducing upper-level divergence–convergence over California; thus, driving the transition between ''dry'' and ''wet'' episodes and the occurrence of extreme rainfall events in the U.S. West Coast. In particular, Mo and Higgins (1998b) pointed out that enhanced tropical convection over the western Pacific (near 150°E) tends to create wet (dry) conditions over the Pacific Northwest and dry (wet) conditions over the Southwest. Jones (2000) and Jones et al. (2004) further showed that extreme precipitation events on both regional (California) and global scales tend to occur more frequently in active MJO phases than in quiescent MJO phases.

The aim of the present study is to 1) quantify the observed Pacific storm-track anomalies during the course of

a typical MJO event, 2) identify the key dynamical processes leading to the storm-track anomalies by diagnosing the synoptic eddy kinetic energy (SEKE) budget, 3) investigate the role of the MJO-induced anomalous synoptic eddy forcing in driving the extratropical intraseasonal flow anomalies, and 4) explore the implications of this storm-track variability for subseasonal prediction of the winter hydrological condition in western North America. Following this introduction, section 2 is a description of the datasets and diagnostic methods used in this study. The development of the storm-track anomalies associated with the intraseasonal variation in tropical convection is presented in section 3, together with a discussion of the potential feedback of storm-track anomalies to tropical outgoing longwave radiation (OLR) variability. The physical processes leading to the storm-track anomalies are examined in section 4 through a SEKE budget analysis with a special emphasis on energy generation due to cross-frequency eddy–eddy interaction (CFEI). Section 5 discusses the role of synoptic eddy forcing in driving the intraseasonal extratropical flow response to MJO and the projection of the storm-track variability onto the subseasonal variation of the winter precipitation over the eastern Pacific and western North America. Conclusions are given in section 6.

2. Data and methods

The analysis of this study focuses on the most recent 30 winters (December–March, 1979/80–2008/09). The main dataset used is the National Centers for Environmental Prediction (NCEP)–National Center for Atmospheric Research (NCAR) reanalysis consisting of standard daily atmospheric fields such as zonal–meridional winds and temperature on 17 pressure levels, precipitable water, and surface precipitation on a 2.5° latitude × 2.5° longitude grid (Kalnay et al. 1996; Kistler et al. 2001). The daily values of the National Oceanic and Atmospheric Administration (NOAA) OLR (Liebmann and Smith 1996) on a 2.5° latitude × 2.5° longitude grid are used as the basis for characterizing intraseasonal variations in the tropical convection.

The synoptic eddy components in various fields are obtained by passing the corresponding daily time series at each grid point through a 2–8-day bandpass Lanczos filter with 17 daily weights (Duchon 1979). The intensity of the North Pacific storm track is then measured in terms of the mass-weighted vertically averaged SEKE between 925 and 200 mb. A 30–90-day bandpass Lanczos filter with 181 daily weights is applied to variables such as daily OLR, SEKE, zonal wind, and precipitation to extract the intraseasonal fluctuations in these fields. The number of weights used in the filter is increased for lower values of cutoff frequencies to ensure a sharp frequency response (Duchon 1979).

A multivariate empirical orthogonal function (MEOF) analysis is conducted on the 30–90-day-filtered daily SEKE (defined over 5°–65°N, 110°E–100°W) and tropical OLR field (defined over 15°S–5°N, 90°E–90°W) to identify the dominant structure of intraseasonal coupling between the North Pacific storm track and tropical convection. The filtered daily SEKE and OLR values at each grid point are first centered (i.e., temporal-mean removed) and normalized, respectively, by the standard deviation of the filtered daily SEKE and OLR time series at the corresponding grid point. The SEKE and OLR fields are then spatially pooled together to form a new data matrix. EOF modes are obtained through eigenvalue decomposition of the correlation matrix derived from the data matrix. The results of the MEOF analysis turn out not sensitive to small changes in the choice of the SEKE and OLR domain.

Composite maps for multiple fields including the SEKE, precipitation, and various local energy conversion terms are created based upon the time series of the principal components (PCs) obtained in the MEOF analysis. A day is denoted as a ''day 0'' when the anomaly of the daily PC value rises above one standard deviation and is greater than the anomaly values of the days immediately preceding and following that day. A total of 52 day 0s are identified out of the 30 winters being studied. This gives us a set of 52 events for case compositing. Composite daily anomalies of various 30–90-day bandpass-filtered fields, that is, composite ''intraseasonal'' anomalies, are constructed from day −30 to day +30 by averaging the corresponding daily fields across the 52 cases selected. Statistical significances of the composites are assessed through Welch's t test (Welch 1947). Two periods characterized by pronounced SEKE response to intraseasonal tropical OLR anomalies are identified through the MEOF analysis and designated as period I and II. They correspond to day −7 to day +7 and day +15 to day +29, respectively. Most results of the composite analysis are presented as averages over each of the two periods.

For the SEKE budget analysis, we derive a SEKE equation with terms of energy generation due to cross-frequency eddy–eddy interaction starting from the horizontal momentum equation of transient eddies in pressure coordinates (e.g., Orlanski and Katzfey 1991; Chang and Orlanski 1993):

$$\frac{\partial \mathbf{V}_T}{\partial t} = -\mathbf{V}_{3\mathrm{M}} \cdot \nabla_3 \mathbf{V}_T - \mathbf{V}_{3\mathrm{T}} \cdot \nabla_3 \mathbf{V}_M - \mathbf{V}_{3\mathrm{T}} \cdot \nabla_3 \mathbf{V}_T - \overline{\mathbf{V}_{3\mathrm{T}} \cdot \nabla_3 \mathbf{V}_T} - \nabla \Phi_T - f\mathbf{k} \times \mathbf{V}_T + \mathbf{F}_{\mathrm{rT}}. \quad (1)$$

In (1), $\mathbf{V}_T$, $\mathbf{V}_M$, $\mathbf{V}_{3\mathrm{T}}$, $\mathbf{V}_{3\mathrm{M}}$ stand for horizontal winds of the transient eddies (departure from time mean), horizontal winds of the time–mean flow, three-dimensional winds (including the vertical velocity) of the transient eddies, and three-dimensional winds of the time-mean flow, respectively. Here, ∇ and ∇_3 represent the two-dimensional and three-dimensional gradient operators, respectively. Here, f, $\mathbf{k}$, Φ_T, and $\mathbf{F}_{\mathrm{rT}}$ are the Coriolis parameter, upward-directed local unit vector, and transient eddy components of geopotential and frictional force, respectively. Overbar in (1) denotes time averaging. We can further decompose the transient winds into three components—namely, the winds associated with high-frequency synoptic eddies (2–8 day) $\mathbf{V}_H$, intermediate-frequency eddies (9–29 day) $\mathbf{V}_I$, and intraseasonal eddies (30–90 day) $\mathbf{V}_L$. By replacing all the variables containing subscripts "T" in (1) with the sum of their corresponding "H", "I," and "L" components (e.g., $\mathbf{V}_T = \mathbf{V}_H + \mathbf{V}_I + \mathbf{V}_L$), rearranging the terms, and applying the 2–8-day bandpass filter to all the terms, we arrive at the momentum equation of synoptic eddies:

$$\frac{\partial \mathbf{V}_H}{\partial t} = -\mathbf{V}_{3\mathrm{M}} \cdot \nabla_3 \mathbf{V}_H - \mathbf{V}_{3\mathrm{H}} \cdot \nabla_3 \mathbf{V}_M - \overline{\mathbf{V}_{3\mathrm{T}} \cdot \nabla_3 \mathbf{V}_T}^H - \nabla \Phi_H - f\mathbf{k} \times \mathbf{V}_H + \mathbf{F}_{\mathrm{rH}}. \quad (2)$$

In (2), overbar with a superscript H denotes 2–8-day bandpass filtering; Φ_H and $\mathbf{F}_{\mathrm{rH}}$ stand for the synoptic eddy components of geopotential and frictional force, respectively.

Taking a dot product of (2) with $\mathbf{V}_H$, making use of the continuity and hydrostatic equation in pressure coordinates and rearranging the terms , we obtain the following SEKE equation:

$$\frac{\partial K_H}{\partial t} = -\nabla_3 \cdot (\mathbf{V}_{3\mathrm{M}} K_H + \Phi_H \mathbf{V}_{3\mathrm{H}}) - \mathbf{V}_H \cdot (\mathbf{V}_{3\mathrm{H}} \cdot \nabla_3 \mathbf{V}_M) - \omega_H \alpha_H - \mathbf{V}_H \cdot \overline{(\mathbf{V}_{3\mathrm{T}} \cdot \nabla_3 \mathbf{V}_T)}^H + \mathbf{F}_{\mathrm{rH}} \cdot \mathbf{V}_H. \quad (3)$$

In (3), K_H is the SEKE, and ω_H and α_H stand for the synoptic eddy components of vertical velocity and specific volume, respectively. On the left-hand side (lhs) of (3) is the local tendency of SEKE. The first term on the right-hand side (rhs) of (3) represents the three-dimensional convergence of energy flux including both time–mean flow advection and dispersion. The second term is the conversion from the time–mean flow kinetic energy to SEKE and is often termed "barotropic conversion." The third term represents the conversion from synoptic eddy potential energy to SEKE, often referred to as "baroclinic conversion". The fourth term corresponds to the generation of SEKE due to cross-frequency eddy–eddy interaction. The last term on the rhs of (3) is the mechanical dissipation associated with friction. Let $\mathbf{V}_T = \mathbf{V}_H + \mathbf{V}_I + \mathbf{V}_L$, $\mathbf{V}_{3\mathrm{T}} = \mathbf{V}_{3\mathrm{H}} + \mathbf{V}_{3\mathrm{I}} + \mathbf{V}_{3\mathrm{L}}$, then we can further decompose the cross-frequency eddy–eddy interaction term in (3) into four parts:

$$-\mathbf{V}_H \cdot \overline{(\mathbf{V}_{3\mathrm{T}} \cdot \nabla_3 \mathbf{V}_T)}^H = -\mathbf{V}_H \cdot \overline{(\mathbf{V}_{3\mathrm{H}} \cdot \nabla_3 \mathbf{V}_H)}^H - \mathbf{V}_H \cdot \overline{(\mathbf{V}_{3\mathrm{H}} \cdot \nabla_3 \mathbf{V}_I + \mathbf{V}_{3\mathrm{I}} \cdot \nabla_3 \mathbf{V}_H + \mathbf{V}_{3\mathrm{I}} \cdot \nabla_3 \mathbf{V}_I)}^H - \mathbf{V}_H \cdot \overline{(\mathbf{V}_{3\mathrm{H}} \cdot \nabla_3 \mathbf{V}_L + \mathbf{V}_{3\mathrm{L}} \cdot \nabla_3 \mathbf{V}_H + \mathbf{V}_{3\mathrm{L}} \cdot \nabla_3 \mathbf{V}_L)}^H - \mathbf{V}_H \cdot \overline{(\mathbf{V}_{3\mathrm{I}} \cdot \nabla_3 \mathbf{V}_L + \mathbf{V}_{3\mathrm{L}} \cdot \nabla_3 \mathbf{V}_I)}^H. \quad (4)$$

The four terms on the rhs of (4) represent the net production of SEKE due to synoptic–synoptic eddy (HH) interaction, synoptic–intermediate-frequency eddy interaction (HI), synoptic–intraseasonal eddy interaction (HL), and the three-way interaction among synoptic, intermediate-frequency, and intraseasonal eddies (HIL), respectively.

3. MJO-induced intraseasonal variation in the Pacific storm track

a. Linear modulation of the Pacific storm track by tropical convection

The linearly covarying patterns of the Pacific storm track and tropical OLR on intraseasonal time scales are first identified through a MEOF analysis on the filtered SEKE and OLR field. The top three EOFs account for, respectively, 11.7%, 8.3%, and 6.4% of the total intraseasonal variance in the two fields. The SEKE and OLR EOFs, in terms of the coefficients of regression onto the corresponding normalized PC time series, are shown in Figs. 1 and 2 , respectively. $\mathrm{EOF1}_{\mathrm{SEKE}}$ (Fig. 1a) has a monopole structure indicating an increase or decrease of the overall intensity of the Pacific storm track. This mode of storm-track variability is largely independent of the tropical OLR as the amplitude of the corresponding $\mathrm{EOF1}_{\mathrm{OLR}}$ (Fig. 2a) is rather weak across the entire tropical region being considered. $\mathrm{EOF2}_{\mathrm{OLR}}$ (Fig. 2b) and $\mathrm{EOF3}_{\mathrm{OLR}}$ (Fig. 2c), on the other hand, indicate an eastward-propagating OLR couplet with the negative anomaly (enhanced convection) located to the west of

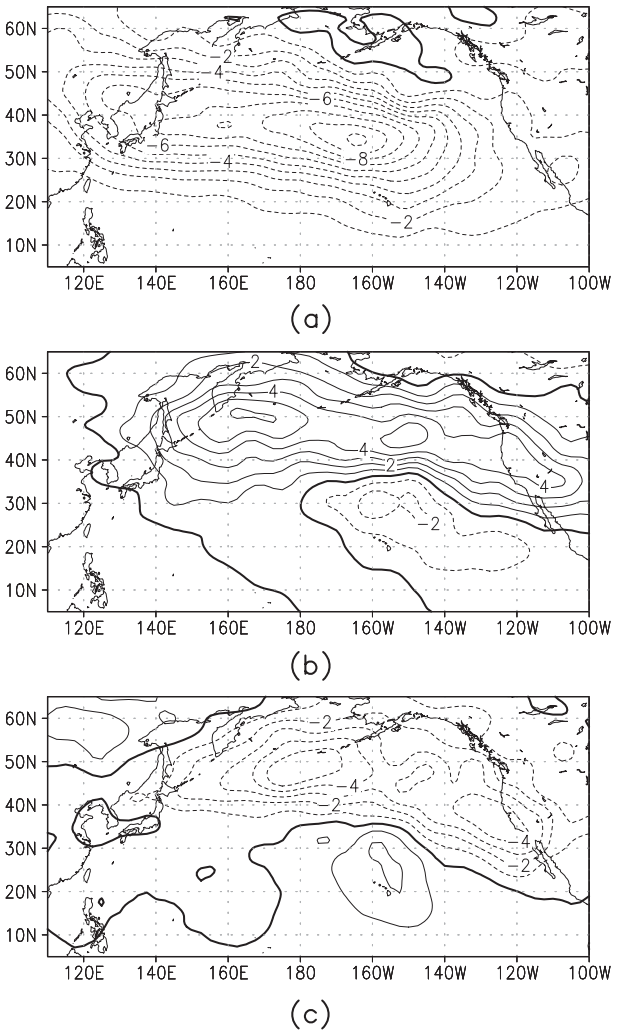

FIG. 1. The first 3 EOF modes of the SEKE shown as the regression coefficients between the intraseasonal SEKE and the corresponding normalized PC time series: (a) $EOF1_{SEKE}$, (b) $EOF2_{SEKE}$, and (c) $EOF3_{SEKE}$. Contour interval is 1 m^2 s^{-2}. Solid (dashed) contours correspond to positive (negative) values and 0 contours are highlighted. Displayed are values reaching the 95% significance level.

the positive anomaly (suppressed convection). The center of the enhanced convection moves from about 110°E in $EOF2_{OLR}$ to about 160°E in $EOF3_{OLR}$. According to the multivariate MJO index defined by Wheeler and Hendon (2004), this movement roughly corresponds to the phase 4–phase 6 evolution of the MJO-related OLR signal over the tropical oceans. The storm-track response, that is, $EOF2_{SEKE}$ (Fig. 1b), is characterized by a dipole anomaly over the North Pacific with above-normal SEKE over mid–high latitudes and below-normal SEKE over the subtropical eastern Pacific. The slightly above-normal SEKE is also observed over the tropical–subtropical central Pacific around the International Date Line. The eastern portions of the storm-track anomalies exhibit a general northwest (NW)–southeast (SE) tilt. In $EOF3_{SEKE}$ (Fig. 1c), the overall distribution of the storm-track anomaly is displaced northeastward compared to $EOF2_{SEKE}$, with a negative anomaly now dominating the mid–high latitudes and a positive anomaly appearing over the subtropical eastern Pacific.

b. *Development of storm-track anomalies and their feedback to tropical OLR*

The development of the storm-track anomalies during the course of a typical MJO event is further examined through case compositing. Day 0s (please refer to the definition in section 2) are selected based upon the second PC (PC2) time series obtained during the MEOF analysis.

Figure 3 illustrates the distributions of the lagged regression coefficients between the intraseasonal tropical OLR anomalies and the normalized PC2 time series. At day −15 (Fig. 3a), a negative OLR anomaly emerges over the Indian Ocean and a positive anomaly appears over the western Pacific. The amplitude of the negative (positive) anomaly increases (decreases) as this OLR couplet propagates eastward between day −15 and day +5 (Figs. 3a–c). By day +15 (Fig. 3d), the positive OLR anomaly has disappeared over the central Pacific and another positive anomaly is found over the Indian Ocean. At day +25 (Fig. 3e), the negative OLR anomaly reaches the central Pacific and is now located south of the equator. The intraseasonal evolution of the tropical OLR associated with the coupled SEKE–OLR variability (PC2) is thus consistent with the life cycle of a typical MJO event (e.g., Fig. 8 of Wheeler and Hendon 2004).

Figure 4 displays the composite intraseasonal anomalies of SEKE for the two periods defined in section 2. Period I (day −7 to day +7, Fig. 4a) is centered about day 0, the time of the peak amplitude of the second EOF mode (Figs. 1b and 2b). During this period, the negative OLR anomaly in the tropics is located over the eastern Indian Ocean and Maritime Continent (Figs. 3b and 3c). The Pacific storm track strengthens across the North Pacific between 35° and 60°N and weakens over the tropical–subtropical eastern Pacific. The slightly enhanced synoptic eddy activity (positive SEKE anomalies) over the tropical–subtropical central Pacific is consistent with the presence of a leakier waveguide over the North Pacific during this stage of MJO as discussed by Matthews and Kiladis (1999). The major difference is here we focus on eddies with shorter time scales (2–8 days versus 6–25 days). As the negative OLR anomaly moves eastward over the equatorial Pacific, the dipole storm-track anomaly of Fig. 4a propagates northeastward and the relative amplitude of the two centers of action also evolves. In period II (day +15–day +29), the center of the enhanced

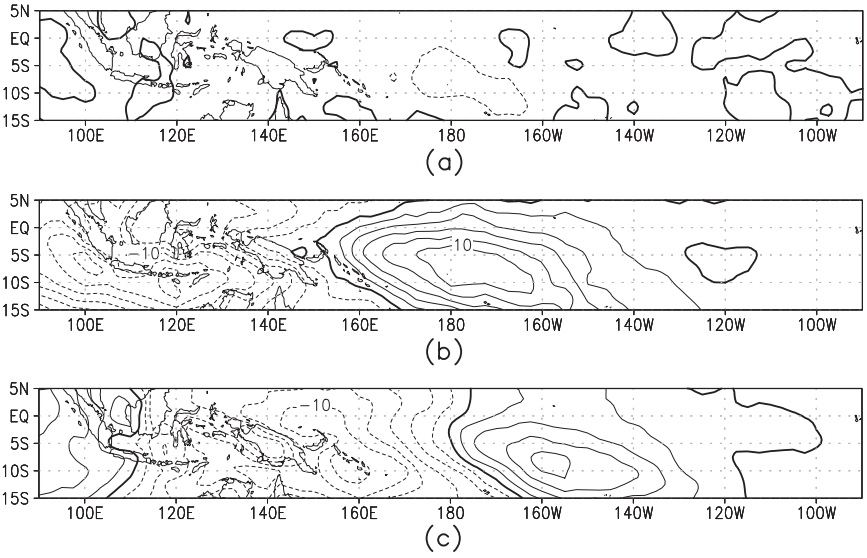

FIG. 2. The first 3 EOF modes of the tropical OLR shown as the regression coefficients between the intraseasonal OLR and the corresponding normalized PC time series: (a) $EOF1_{OLR}$, (b) $EOF2_{OLR}$, and (c) $EOF3_{OLR}$. Contour interval is 2 W m^{-2}. Solid (dashed) contours correspond to positive (negative) values and 0 contours are highlighted. Displayed are values reaching the 95% significance level.

tropical convection is now over the tropical western-central Pacific (Figs. 3d and 3e). The corresponding SEKE field (Fig. 4b) now indicates largely suppressed synoptic eddy activity (negative SEKE anomalies) north of 35°N and enhanced eddy activity over the tropical–subtropical eastern Pacific. The overall anomaly distribution is almost the same compared to that in period I (Fig. 4a) but with opposite signs. Over the tropical–subtropical central Pacific, the SEKE anomalies are weakly negative at this stage, which is in contrast with the positive values found in period I. The similarities between the period I (II) SEKE composite and the $EOF2(3)_{SEKE}$ demonstrate that 1) the second and third EOF mode indeed reflect, respectively, two consecutive stages during the intraseasonal coupling between the SEKE and tropical OLR, and 2) the response of the North Pacific storm track to the intraseasonal variation in tropical convection is largely linear. In general, this intraseasonal modulation can be described as a northeastward-propagating, amplitude-varying dipole anomaly in the SEKE field. If counting in the weak yet distinct anomalies over the tropical–subtropical central Pacific, the anomalous synoptic eddy activity over the North Pacific is characterized by a tripole pattern.

To explore the potential feedback of storm-track anomalies to tropical convection, we document the temporal evolution of the meridional propagation of synoptic eddy energy across a subtropical zone (15°–20°N) and compare this evolution to that of the synoptic variability in the tropical (0°–15°N) OLR during the course of an MJO event. The direction of eddy group velocity is approximately quantified by the barotropic **E** vector, $\mathbf{E} = (E_x, E_y) = (\overline{v'^2} - \overline{u'^2}, -\overline{u'v'})$, where u' and v' are the synoptic eddy component of the zonal and meridional wind, respectively, and overbar indicates time averaging (Hoskins et al. 1983). Figure 5a is a longitude–time plot showing the anomalies of the 2–8-day bandpass-filtered tropical OLR variance (contour) between day −15 and day +30 together with the corresponding anomalies of the meridional component of the 250-mb **E** vector (E_y) averaged over 15°–20°N (color shading). Between 140° and 170°E, during the period day −15 to day +10, the equatorward propagation of synoptic eddy energy (negative values of E_y) leads an enhancement of the tropical OLR variability by about 3–5 days. After day +10, the sign of E_y changes and poleward propagation of eddy energy is now evident across the subtropics between 140° and 170°E. This propagation also slightly leads the suppressed tropical OLR variability between day +12 and day +30. In Fig. 5b, the tropical OLR variance is replaced with the 30–90-day bandpass-filtered OLR anomalies. A comparison between Figs. 5a and 5b indicates that enhanced (suppressed) synoptic variability of OLR is typically associated with negative (positive) intraseasonal anomalies of OLR except for a region around 170°E between day +10 and day +25. The equatorward propagation of the synoptic eddy energy identified between day −15 and day +10 over 140°–170°E thus suggests a positive feedback of the storm-track response to

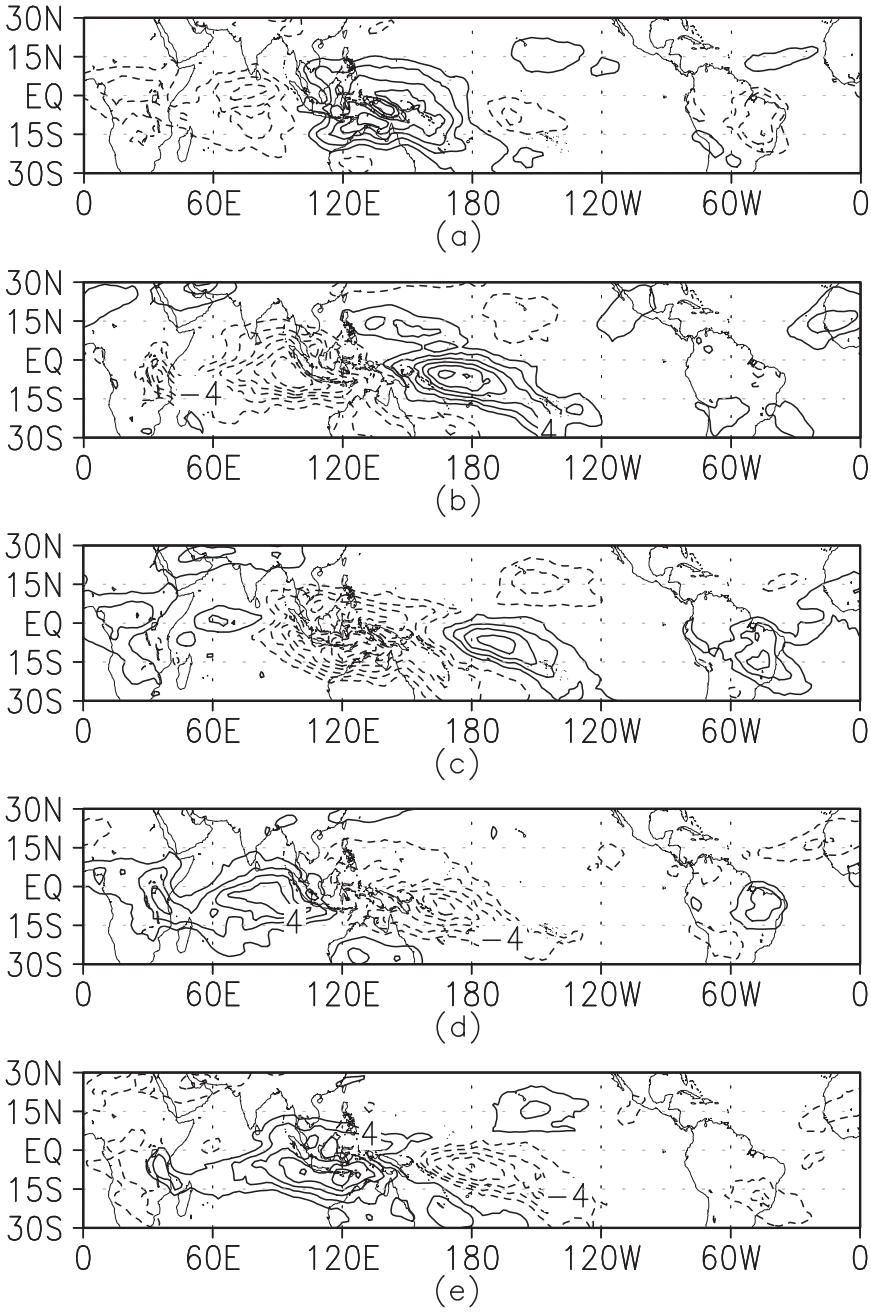

FIG. 3. The distribution of the lagged regression coefficients between the intraseasonal tropical OLR anomalies and the normalized PC2 time series at (a) day −15, (b) day −5, (c) day +5, (d) day +15, and (e) day +25. Contour interval is 2 W m^{-2}. Solid (dashed) contours correspond to positive (negative) values and 0 contours are omitted. Displayed are values reaching the 95% significance level.

the eastward advance of the MJO-related OLR signal in the tropics, in terms of both its synoptic variability and intraseasonal anomalies. Similar behavior for transient eddies with lower frequencies was discussed by Matthews and Kiladis (1999). No distinct feedback process is found for longitudes east of 170°E or after day +10.

4. Energetic processes contributing to storm-track anomalies

The local SEKE budget is analyzed with Eq. (3) and (4) to identify the key energetic processes contributing to the composite anomalies of SEKE in periods I and II

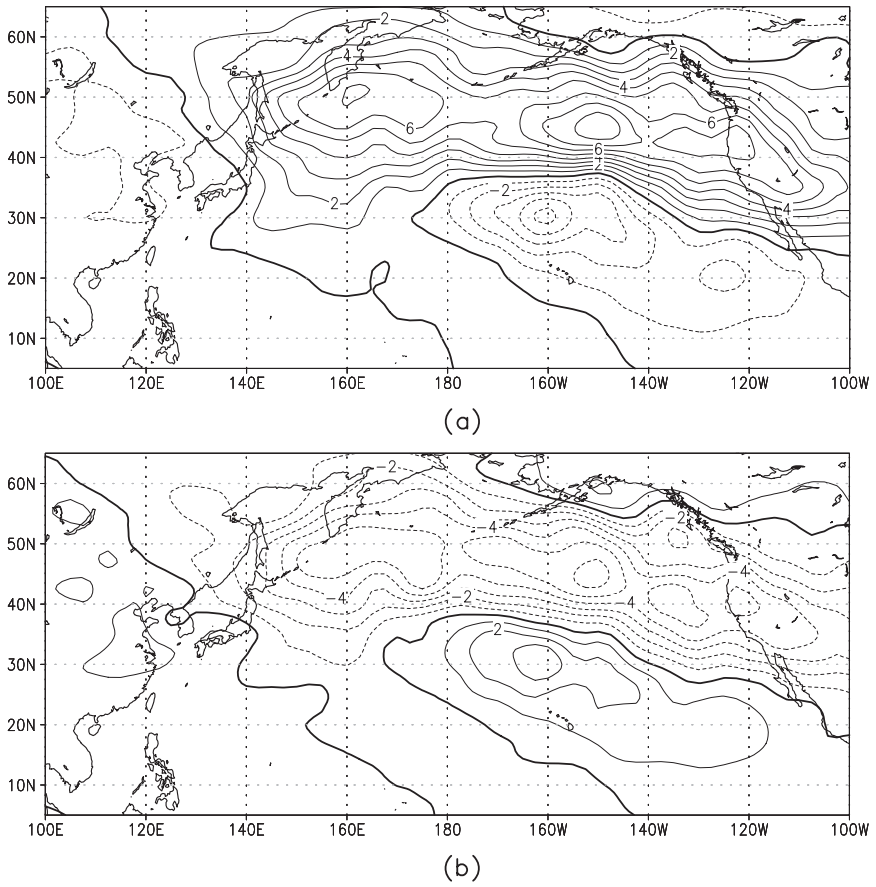

FIG. 4. Composite intraseasonal storm-track anomalies in terms of the vertically (925–200 mb) averaged SEKE during (a) period I (b) and period II. Please refer to the text for the definition of the 2 periods. Contour interval is 1 m^2 s^{-2}. Solid (dashed) contours correspond to positive (negative) values and 0 contours are highlighted. Displayed are values reaching the 95% significance level.

(Fig. 4). The discussion is focused on the four main conversion terms on the rhs of (3)—namely, the energy flux convergence (EFC), barotropic conversion (BT), baroclinic conversion (BC), and the generation of SEKE due to CFEI. The CFEI term is further decomposed into HH, HI, HL, and HIL (please refer to the definitions in section 2) to identify the most important component of the cross-frequency eddy–eddy interaction. Since energy conversion terms represent only the ''tendency'' of the local SEKE, the composite intraseasonal anomalies of these terms are time shifted and constructed for periods preceding previously defined periods I and II. Specifically, the energy composites for period I (II) are averages over day −12 to day +2 (day +10–day +24) and are shown in Fig. 6 (Fig. 7). Figures 6a–e correspond to the mean SEKE tendency, EFC, BT, BC, and CFEI, respectively. The mean SEKE tendency in Fig. 6a has a distribution very similar to that of the SEKE anomalies of period I shown in Fig. 4a, which demonstrates that the choice of the averaging period for energy conversion terms is appropriate. The magnitudes of the anomalies of EFC, BC, and CFEI are comparable, indicating equally important contributions to the SEKE tendency by all three processes. It is also worth noting that the values of the individual conversion terms are typically an order of magnitude larger than those of the mean SEKE tendency, implying substantial cancellations among various conversion terms.

In Fig. 6a, an above-normal growth rate of SEKE is found north of 40°N, extending from the northwestern North Pacific to western North America. This above-normal growth is collectively contributed by positive anomalies of BC over the northwestern North Pacific east of Japan (Fig. 6d), positive anomalies of CFEI over the eastern Pacific (Fig. 6e), and positive anomalies of EFC over western North America (Fig. 6b). The below-normal growth rate of SEKE over the subtropical eastern Pacific is largely associated with the negative BC

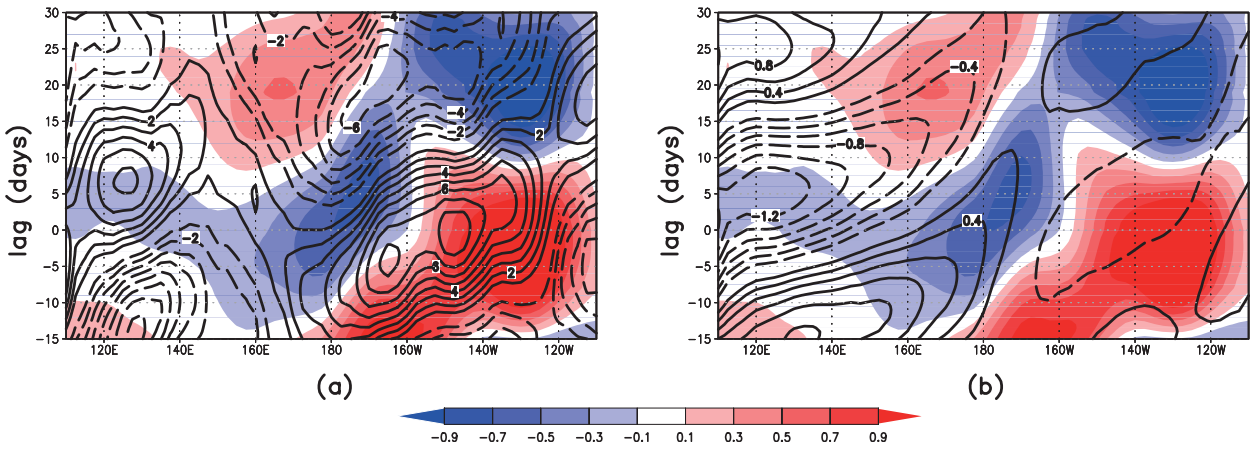

FIG. 5. (a) Longitude–time plot of the composite intraseasonal anomalies of the 2–8-day bandpass-filtered OLR variance (contours) averaged over 0°–15°N and the composite intraseasonal anomalies of E_y (color shading) averaged over 15°–20°N. (b) As in (a), but for the contours now corresponding to the composite intraseasonal (30–90-day bandpass-filtered) anomalies of the OLR averaged over 0°–15°N. Contour interval is 1 W^2 m^{-4} in (a) and 0.2 W m^{-2} in (b). Solid (dashed) contours correspond to positive (negative) values and 0 contours are omitted. Unit for the color shading is m^2 s^{-2}. Please refer to the text for the definition of day 0.

anomalies over 180°–130°W (Fig. 6d) with secondary contributions from EFC (around 140°W, 25°N, Fig. 6b) and CFEI (around 130°W, 20°N, Fig. 6e). The BT anomalies (Fig. 6c) are concentrated around 40°N, generally negative, and have smaller amplitudes compared to other conversion terms. They have minor negative (positive) contributions to the SEKE tendency north (south) of 40°N. After comparing the four components of the eddy–eddy interaction term (i.e., HH, HI, HL, and HIL), we found that the interaction between synoptic eddies and HL dominates the CFEI anomalies seen in Fig. 6e. Shown in Fig. 6f, the distribution of HL anomalies is approximately characterized by a dipole structure in the zonal direction across the midlatitude North Pacific. It indicates that substantial amounts of SEKE are generated (lost) through the interaction between the synoptic eddy and intraseasonal eddy component of the flow over the eastern Pacific (western-central Pacific).

The mean SEKE tendency in Fig. 7a is also consistent with the SEKE anomalies observed during period II (Fig. 4b). Similar to the previous period, the below-normal growth rate north of 40°N is contributed by negative BC anomalies (Fig. 7d) over the northwestern North Pacific, negative CFEI anomalies over the eastern Pacific (Fig. 7e), and negative EFC anomalies over the eastern Pacific–western North America (Fig. 7b). The enhanced SEKE growth south of 40°N is primarily associated with positive BC anomalies over 180°–130°W (Fig. 7d) and positive EFC anomalies over 160°–110°W (Fig. 7b). The BT anomalies are again weaker compared to other conversion terms and have minor negative (positive) contributions to the SEKE tendency north (south) of 40°N (Fig. 7c). During this stage, CFEI (Fig. 7e) is also dominated by HL (Fig. 7f) with the signs of the zonal dipole reversed compared to the previous stage (Fig. 6f). Significant loss of SEKE due to the interaction between synoptic eddies and intraseasonal flow is now seen over the eastern Pacific.

From Figs. 6 and 7, we may conclude that the storm-track response to intraseasonal variation in tropical convection is generated through nearly equally important changes in the convergence of energy flux, baroclinic conversion, and SEKE generation due to the interaction between synoptic eddies and intraseasonal flow. Both the magnitudes and signs of these three terms have large spatial variations and also evolve during the course of a typical MJO event. Among these processes, EFC and CFEI are, respectively, linked to the properties of a wintertime–mean flow and intraseasonal flow anomalies that often appear in the form of barotropic Rossby waves forced directly by anomalous tropical heating (e.g., Matthews et al. 2004). The significant contribution of HL to the SEKE anomalies thus suggests the importance of the ''direct'' extratropical response to MJO variability in setting up the storm-track anomalies associated with the MJO. The SEKE budget analysis done here serves a first step toward understanding the rather complicated processes of eddy–mean flow interaction and eddy–eddy interaction involved in the development of the extratropical response to MJO variability.

5. Synoptic eddy feedback to intraseasonal flow and precipitation

In this section, we examine how the storm-track anomalies induced by variation in tropical convection feedback to the intraseasonal flow anomalies over the North Pacific

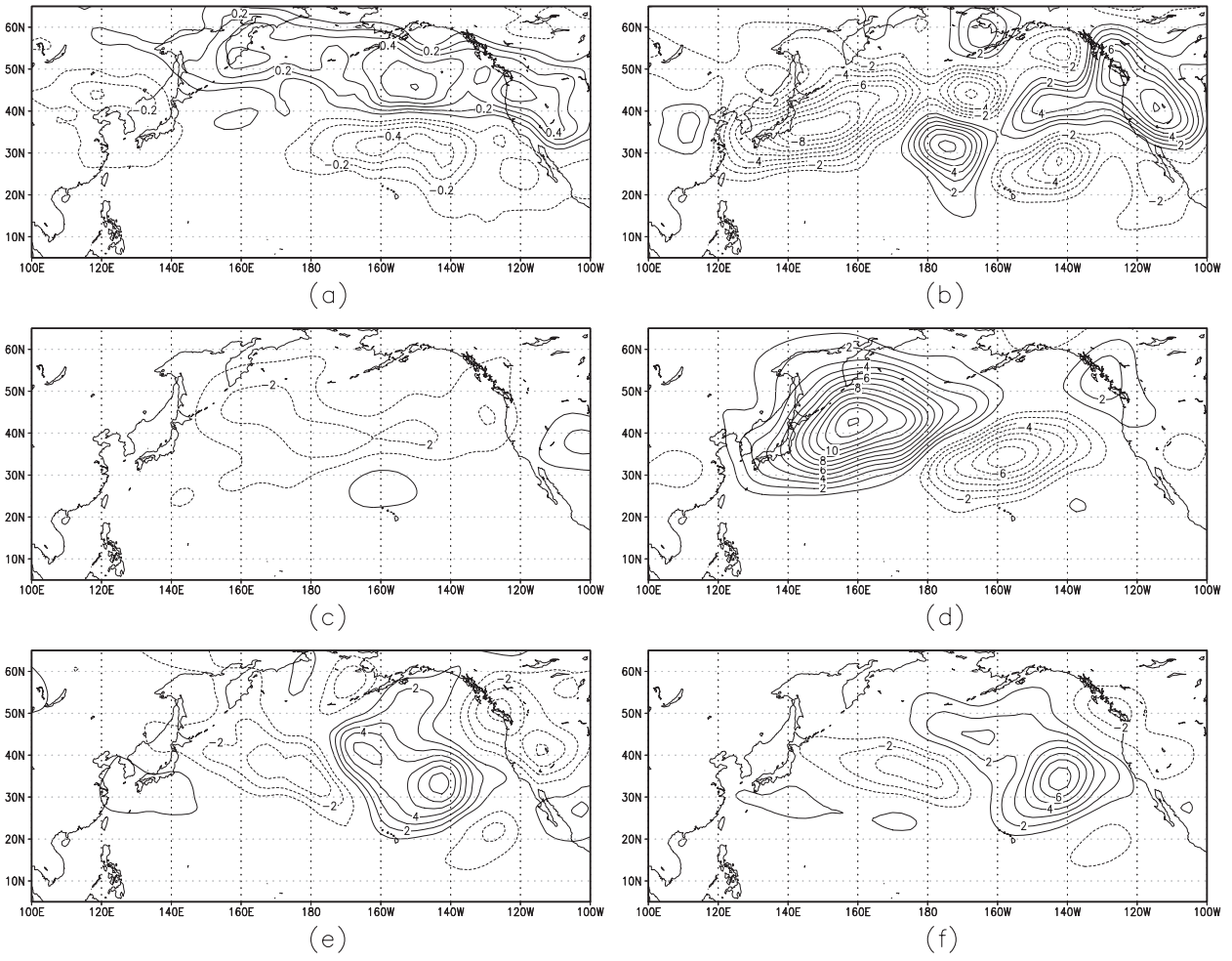

FIG. 6. Composite intraseasonal anomalies of the (a) SEKE tendency, (b) EFC, (c) BT, (d) BC, (e) CFEI, and (f) HL for the period (day −12 to day +2) relevant to period I SEKE anomalies. Contour interval is 0.1 $m^2\ s^{-2}\ day^{-1}$ for (a) and 1 $m^2\ s^{-2}\ day^{-1}$ for the rest. Solid (dashed) contours correspond to positive (negative) values and 0 contours are omitted. Displayed are values reaching the 95% significance level.

and meanwhile generate low-frequency variability in the hydrological conditions over the eastern Pacific and western North America. The anomalous intraseasonal (30–90-day bandpass-filtered) zonal wind (contour) at 250 mb is shown in Figs. 8a and 8b for periods I and II, respectively. Superimposed on the zonal wind anomalies are the corresponding intraseasonal anomalies of the barotropic **E** vector (arrow) and their divergence (color shading) that quantifies the westerly acceleration of intraseasonal flow due to synoptic eddy forcing (Hoskins et al. 1983). During period I, the zonal wind anomalies are characterized by anomalous westerlies north of 40°N and south of 20°N over the North Pacific with anomalous easterlies dominating 20°–40°N. This distribution of zonal wind anomalies corresponds to an anticyclonic circulation anomaly centered about 40°N and, to its south, a cyclonic circulation anomaly centered about 20°N. The NW–SE tilt of the anticyclone and cyclone suggests that these are Rossby waves driven primarily by the anomalous tropical cooling (positive OLR anomaly) present over the central Pacific in period I (see Figs. 3b and 3c). The divergence (convergence) of **E** vectors near 50°N, 160°W (35°N, 160°W), however, indicates pronounced westerly (easterly) acceleration due to anomalous synoptic eddy forcing. The collocation of the westerly (easterly) acceleration due to synoptic eddy forcing and the westerly (easterly) intraseasonal flow anomalies, particularly over the eastern and northern portion of the anticyclone, suggests a positive feedback of storm-track response to the anticyclonic circulation anomaly over the North Pacific. During period II (Fig. 8b), a cyclonic circulation anomaly is found north of an anticyclonic anomaly. They are largely forced by the anomalous tropical heating (negative OLR anomaly) over the central

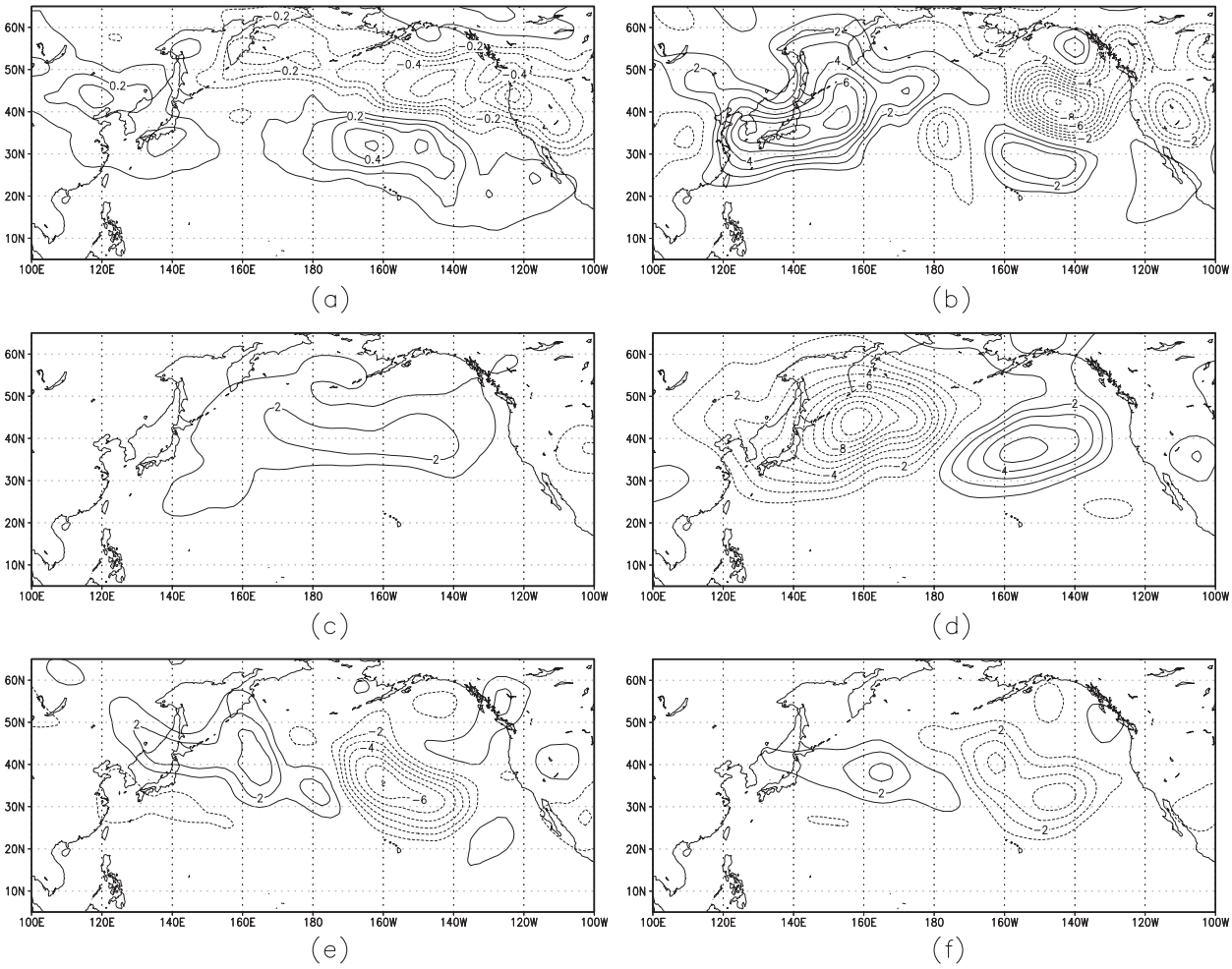

FIG. 7. As in Fig. 6, but for the period (day +10–day +24) relevant to period II SEKE anomalies.

Pacific (see Figs. 3d and 3e), but the synoptic eddy forcing still contributes significantly to the wind anomalies over the eastern and northern portion of the cyclone.

Coastal cyclonic activity in winter largely determines the year-to-year fluctuations in the precipitation characteristics over the western United States. (Myoung and Deng 2009). Here, as an initial effort to assess the subseasonal downstream control of the Pacific storm track on the western U.S. hydrological conditions, we compare the temporal evolutions of the intraseasonal anomalies of precipitable water and SEKE over eastern North Pacific–western North America during the course of an MJO event. Figure 9a is a time–latitude plot showing the precipitable water (contour) and SEKE (color shading) anomalies averaged over 135°–120°W. The total moisture content over this region is characterized by a three-band anomaly (dry–wet–dry) propagating poleward from day −30 to day +30. The moisture anomalies are largely in phase with those of SEKE, demonstrating the important role played by synoptic eddies in the meridional moisture transport in the extratropics (e.g., Peixoto and Oort 1992). The three-band anomaly is also evident in the surface precipitation (Fig. 9b). The SEKE and precipitation anomalies are nearly in phase north of 40°N, that is, above (below) normal precipitation corresponds to enhanced (suppressed) SEKE. Around 32°N, the precipitation anomaly attains its maximum amplitude about 3–5 days before the arrival of the maximum amplitude of the SEKE anomaly, indicating that a substantial amount of rainfall in this region occurs ahead (east) of the center and in the warm sector of a coastal cyclone. Because of the modulation of the synoptic eddy activity of the Pacific storm track, the eastern Pacific and the coastal region of western North America between 25° and 40°N experiences a transition around day −5 from a wet to a dry regime and each regime lasts approximately 25 days (Fig. 9b). North of 40°N, two transitions, dry to wet and wet to dry, occur around day −10 and day +15, respectively.

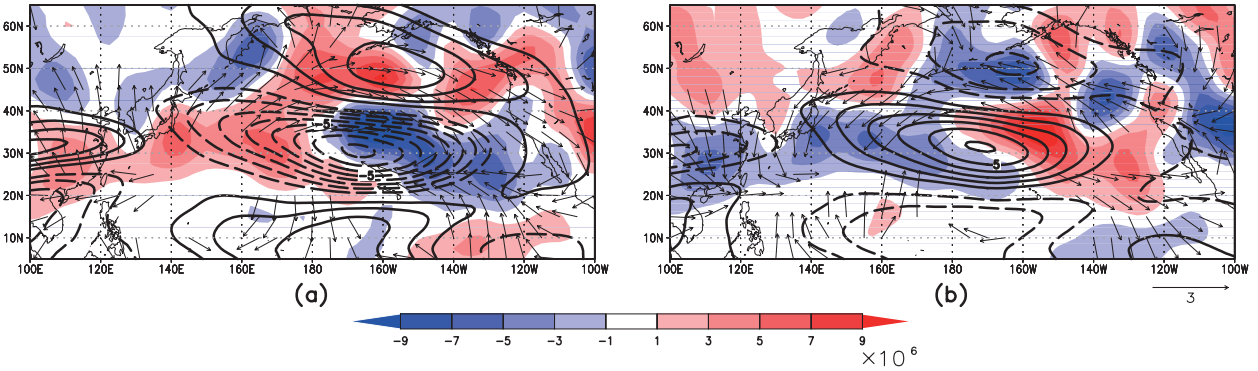

FIG. 8. Composite intraseasonal anomalies of the zonal wind (contour), barotropic **E** vector (arrow), and divergence of **E** vector (color shading) at 250 mb during (a) period I and (b) period II. Contour interval is 1 m s^{-1}. Solid (dashed) contours correspond to positive (negative) values and 0 contours are omitted. The **E** vectors are plotted if either (x or y) component is statistically significant at the 95% level; and they have been normalized to unit length to focus on the direction. Unit for the color shading is m s^{-2}.

6. Conclusions

This diagnostic study examines the response of the Pacific storm track to the intraseasonal variation in tropical convection characteristic of a typical MJO event in boreal winter. A MEOF analysis conducted on the 30–90-day bandpass-filtered tropical OLR and mass-weighted, vertically-averaged SEKE field reveals a pronounced dipole anomaly of the Pacific storm track propagating northeastward as an OLR couplet moves from the east Indian Ocean to the western-central Pacific. This movement roughly corresponds to the phase 4–phase 6 evolution of MJO according to the multivariate MJO index defined by Wheeler and Hendon (2004). We further divide the development of the storm-track response into two periods with period I and II corresponding to the days when the center of enhanced tropical convection (largest negative OLR anomalies) is located over the eastern Indian Ocean–Maritime Continent and the equatorial western-central Pacific, respectively. Case compositing for the SEKE anomalies during these two periods confirms that the storm-track response to the intraseasonal variation in tropical convection can be described as a northeastward-propagating, amplitude-varying dipole anomaly in the

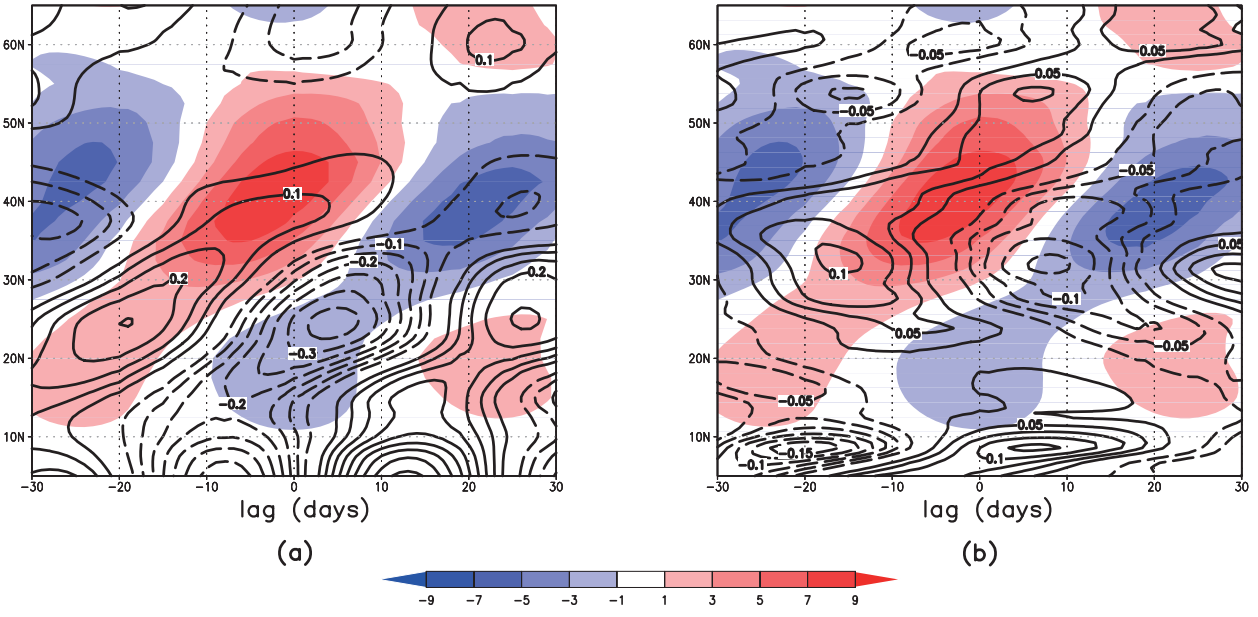

FIG. 9. (a) Time–latitude plot of the composite intraseasonal anomalies of precipitable water (contours) and SEKE (color shading) averaged over 135°–120°W. (b) As in (a), but the contours now correspond to the composite intraseasonal anomalies of precipitation. Contour interval is 0.05 mm in (a) and 0.025 mm day^{-1} in (b). Solid (dashed) contours correspond to positive (negative) values and 0 contours are omitted. Unit for the color shading is m^2 s^{-2}.

SEKE field. A tripole anomaly pattern in the North Pacific SEKE field is identified if counting in the weak yet distinct SEKE anomalies found over the tropical–subtropical central Pacific. During period I, over 140°–170°E, the anomalous equatorward propagation of transient energy over a subtropical zone (15°–20°N) contributes to a higher level of synoptic variability in the tropical OLR, which projects into the negative, eastward-propagating intraseasonal anomalies of the OLR. This constitutes a positive feedback of storm-track response to MJO-related variability in tropical convection.

A diagnosis of the local SEKE budget shows that three energy conversion processes (i.e., convergence of energy flux, baroclinic conversion, and generation of SEKE due to interaction between synoptic eddies and intraseasonal flow) are nearly equally important in terms of contributing to the SEKE anomalies observed during the two periods. The relative magnitude and spatial distributions of these three conversion terms also evolve during the course of an MJO event. This budget analysis demonstrates significant roles played by eddy–mean flow interaction and eddy–eddy interaction in the development of the extratropical response to MJO variability. Accompanying the evolution of the tropical OLR, an anticyclonic (cyclonic) circulation anomaly in the upper-tropospheric intraseasonal flow, and to its south, a cyclonic (anticyclonic) circulation anomaly, develops over the North Pacific during period I (period II). The anticyclonic (cyclonic) circulation anomaly found during period I (period II) is part of a Rossby wave train forced primarily by anomalous tropical heating associated with the MJO. The eastern and northern portions of these circulation anomalies, however, are partly maintained by the anomalous synoptic eddy forcing that is quantified in terms of the divergence–convergence of the barotropic **E** vector. The last part of the analysis is an initial effort to quantify the subseasonal, dynamical control of the Pacific storm track on the hydroclimate variability over its downstream region. Associated with the SEKE anomalies identified here, a three-band (dry–wet–dry) precipitation anomaly forms and propagates poleward over the eastern Pacific and the coastal region of western North America during the course of an MJO event. The region between 25° and 40°N makes a transition from a wet to a dry regime around day −5 (i.e., when the center of enhanced tropical convection reaches 110°E), with each regime lasting approximately 25 days. North of 40°N, two transitions occur at day −10 and day +15, respectively. Future research efforts will include a quantification of the predictive skill resulting from the storm-track modulation of the subseasonal hydroclimate variability in western North America.

Acknowledgments. We thank three anonymous reviewers for their thoughtful comments and suggestions that led to major improvements of the manuscript. The NCEP–NCAR reanalysis and NOAA OLR data used in this study were provided through the NOAA Climate Diagnostics Center. This research was supported by NASA Energy and Water Cycle Study (NEWS) under Grant NNX09AJ36G.

REFERENCES

Black, R. X., 1997: Deducing anomalous wave source regions during the life cycles of persistent flow anomalies. *J. Atmos. Sci.,* **54,** 895–907.

Blackmon, M. L., 1976: A climatological spectral study of the 500-mb geopotential height of the Northern Hemisphere. *J. Atmos. Sci.,* **33,** 1607–1623.

——, J. M. Wallace, N. C. Lau, and S. L. Mullen, 1977: An observational study of the Northern Hemisphere wintertime circulation. *J. Atmos. Sci.,* **34,** 1040–1053.

Cai, M., and M. Mak, 1990: Symbiotic relation between planetary- and synoptic-scale waves. *J. Atmos. Sci.,* **47,** 2953–2968.

Chang, E. K. M., 2001: GCM and observational diagnoses of the seasonal and interannual variations of the Pacific storm track during the cool season. *J. Atmos. Sci.,* **58,** 1784–1800.

——, 2003: Midwinter suppression of the Pacific storm-track activity as seen in aircraft observations. *J. Atmos. Sci.,* **60,** 1345–1358.

——, 2007: Assessing the increasing trend in Northern Hemisphere winter storm-track activity using surface ship observations and a statistical storm-track model. *J. Climate,* **20,** 5607–5628.

——, and I. Orlanski, 1993: On the dynamics of a storm track. *J. Atmos. Sci.,* **50,** 999–1015.

——, and Y. Fu, 2002: Interdecadal variations in Northern Hemisphere winter storm-track intensity. *J. Climate,* **15,** 642–658.

——, S. Lee, and K. L. Swanson, 2002: Storm-track dynamics. *J. Climate,* **15,** 2163–2183.

Deng, Y., and M. Mak, 2005: An idealized model study relevant to the dynamics of the midwinter minimum of the Pacific storm track. *J. Atmos. Sci.,* **62,** 1209–1225.

——, and ——, 2006: Nature of the differences in the intraseasonal variability of the Pacific and Atlantic storm tracks: A diagnostic study. *J. Atmos. Sci.,* **63,** 2602–2615.

Dole, R. M., and N. D. Gordon, 1983: Persistent anomalies of the extratropical Northern Hemisphere wintertime circulation: Geographical distribution and regional persistence characteristics. *Mon. Wea. Rev.,* **111,** 1567–1586.

——, and R. X. Black, 1990: Life cycles of persistent anomalies. Part II: The development of persistent negative height anomalies over the North Pacific Ocean. *Mon. Wea. Rev.,* **118,** 824–846.

Duchon, C. E., 1979: Lanczos filtering in one and two dimensions. *J. Appl. Meteor.,* **18,** 1016–1022.

Egger, J., and K. M. Weickmann, 2007: Latitude–height structure of the atmospheric angular momentum cycle associated with the Madden–Julian oscillation. *Mon. Wea. Rev.,* **135,** 1564–1575.

Gerber, E. P., and G. K. Vallis, 2009: On the zonal structure of the North Atlantic oscillation and annular modes. *J. Atmos. Sci.,* **66,** 332–352.

Held, I. M., S. W. Lyons, and S. Nigam, 1989: Transients and the extratropical response to El Niño. *J. Atmos. Sci.,* **46,** 163–174.

Higgins, R. W., and K. C. Mo, 1997: Persistent North Pacific circulation anomalies and the tropical intraseasonal oscillation. *J. Climate,* **10,** 223–244.

——, J.-K. E. Schemm, W. Shi, and A. Leetmaa, 2000: Extreme precipitation events in the western United States related to tropical forcing. *J. Climate,* **13,** 793–820.

Hoerling, M. P., and M. Ting, 1994: Organization of extratropical transients during El Niño. *J. Climate,* **7,** 745–766.

Holopainen, E. O., 1990: Role of cyclone-scale eddies in the general circulation of the atmosphere: A review of recent observational studies. *Extratropical Cyclones: The Erik Palmen Memorial Volume,* C. W. Newton and E. O. Holopainen, Eds., Amer. Meteor. Soc., 48–62.

Horel, J. D., and J. M. Wallace, 1981: Planetary-scale atmospheric phenomena associated with the Southern Oscillation. *Mon. Wea. Rev.,* **109,** 813–829.

Hoskins, B. J., and T. Ambrizzi, 1993: Rossby wave propagation on a realistic longitudinally varying flow. *J. Atmos. Sci.,* **50,** 1661–1671.

——, and G.-Y. Yang, 2000: The equatorial response to higher-latitude forcing. *J. Atmos. Sci.,* **57,** 1197–1213.

——, I. N. James, and G. H. White, 1983: The shape, propagation, and mean-flow interaction of large-scale weather systems. *J. Atmos. Sci.,* **40,** 1595–1612.

Jones, C., 2000: Occurrence of extreme precipitation events in California and relationships with the Madden–Julian oscillation. *J. Climate,* **13,** 3576–3587.

——, D. E. Waliser, K. M. Lau, and W. Stern, 2004: Global occurrences of extreme precipitation and the Madden–Julian oscillation: Observations and predictability. *J. Climate,* **17,** 4575–4589.

Kalnay, E., and Coauthors, 1996: The NCEP/NCAR 40-Year Reanalysis Project. *Bull. Amer. Meteor. Soc.,* **77,** 437–471.

Kiladis, G. N., 1998: Observations of Rossby waves linked to convection over the eastern tropical Pacific. *J. Atmos. Sci.,* **55,** 321–339.

——, and K. M. Weickmann, 1992a: Circulation anomalies associated with tropical convection during northern winter. *Mon. Wea. Rev.,* **120,** 1900–1923.

——, and ——, 1992b: Extratropical forcing of tropical pacific convection during northern winter. *Mon. Wea. Rev.,* **120,** 1924–1939.

Kistler, R., and Coauthors, 2001: The NCEP–NCAR 50–Year Reanalysis: Monthly means CD–ROM and documentation. *Bull. Amer. Meteor. Soc.,* **82,** 247–267.

Lau, N. C., 1988: Variability of the observed midlatitude storm tracks in relation to low-frequency changes in the circulation pattern. *J. Atmos. Sci.,* **45,** 2718–2743.

Liebmann, B., and C. A. Smith, 1996: Description of a complete (interpolated) outgoing longwave radiation dataset. *Bull. Amer. Meteor. Soc.,* **77,** 1275–1277.

Lin, H., G. Brunet, and J. Derome, 2009: An observed connection between the North Atlantic Oscillation and the Madden–Julian oscillation. *J. Climate,* **22,** 364–380.

Madden, R. A., and P. R. Julian, 1972: Description of global-scale circulation cells in the tropics with a 40–50-day period. *J. Atmos. Sci.,* **29,** 1109–1123.

——, and ——, 1994: Observations of the 40–50-day tropical oscillation—A review. *Mon. Wea. Rev.,* **122,** 814–837.

Mak, M. K., 1969: Laterally driven stochastic motions in the tropics. *J. Atmos. Sci.,* **26,** 41–64.

Matthews, A. J., and G. N. Kiladis, 1999: The tropical–extratropical interaction between high-frequency transients and the Madden–Julian oscillation. *Mon. Wea. Rev.,* **127,** 661–677.

——, B. J. Hoskins, and M. Masutani, 2004: The global response to tropical heating in the Madden–Julian oscillation during the northern winter. *Quart. J. Roy. Meteor. Soc.,* **130,** 1991–2011.

Mo, K. C., 1999: Alternating dry and wet episodes over California and intraseasonal oscillations. *Mon. Wea. Rev.,* **127,** 2759–2776.

——, and R. E. Livezey, 1986: Tropical–extratropical geopotential height teleconnections during the Northern Hemisphere winter. *Mon. Wea. Rev.,* **114,** 2488–2515.

——, and R. W. Higgins, 1998a: Tropical influences on California precipitation. *J. Climate,* **11,** 412–430.

——, and ——, 1998b: Tropical convection and precipitation regimes in the western United States. *J. Climate,* **11,** 2404–2423.

Myoung, B., and Y. Deng, 2009: Interannual variability of the cyclonic activity along the U.S. Pacific Coast: Influences on the characteristics of winter precipitation in the western United States. *J. Climate,* **22,** 5732–5747.

Nakamura, H., 1992: Midwinter suppression of baroclinic wave activity in the Pacific. *J. Atmos. Sci.,* **49,** 1629–1642.

——, T. Izumi, and T. Sampe, 2002: Interannual and decadal modulations recently observed in the pacific storm-track activity and East Asian winter monsoon. *J. Climate,* **15,** 1855–1874.

Orlanski, I., and J. Katzfey, 1991: The life cycle of a cyclone wave in the Southern Hemisphere. Part I: Eddy energy budget. *J. Atmos. Sci.,* **48,** 1972–1998.

Pan, L., and T. Li, 2008: Interaction between the tropical ISO and midlatitude low-frequency flow. *Climate Dyn.,* **31,** 375–388.

Peixoto, J. P., and A. H. Oort, 1992: *Physics of Climate*. American Institute of Physics, 520 pp.

Penny, S., G. H. Roe, and D. S. Battisti, 2010: The source of the midwinter suppression in storminess over the North Pacific. *J. Climate,* **23,** 634–648.

Rauber, R. M., J. E. Walsh, and D. J. Charlevoix, 2008: *Severe and Hazardous Weather: An Introduction to High-Impact Meteorology*. 3rd ed. Kendall/Hunt Publishing Company, 642 pp.

Rivière, G., and I. Orlanski, 2007: Characteristics of the Atlantic storm-track eddy activity and its relation with the North Atlantic Oscillation. *J. Atmos. Sci.,* **64,** 241–266.

Straus, D. M., and R. S. Lindzen, 2000: Planetary-scale baroclinic instability and the MJO. *J. Atmos. Sci.,* **57,** 3609–3626.

——, and J. Shukla, 1997: Variations of midlatitude transient dynamics associated with ENSO. *J. Atmos. Sci.,* **54,** 777–790.

——, and ——, 2002: Does ENSO Force the PNA? *J. Climate,* **15,** 2340–2358.

Tomas, R. A., and P. J. Webster, 1994: Horizontal and vertical structure of cross-equatorial wave propagation. *J. Atmos. Sci.,* **51,** 1417–1430.

Trenberth, K. E., 1986: An assessment of the impact of transient eddies on the zonal flow during a blocking episode using localized Eliassen–Palm flux diagnostics. *J. Atmos. Sci.,* **43,** 2070–2087.

——, and J. W. Hurrell, 1994: Decadal atmosphere–ocean variations in the Pacific. *Climate Dyn.,* **9,** 303–319.

Wallace, J. M., and D. S. Gutzler, 1981: Teleconnections in the geopotential height field during the Northern Hemisphere winter. *Mon. Wea. Rev.,* **109,** 784–812.

Weickmann, K. M., 1983: Intraseasonal circulation and outgoing longwave radiation modes during Northern Hemisphere winter. *Mon. Wea. Rev.,* **111,** 1838–1858.

——, G. R. Lussky, and J. E. Kutzbach, 1985: Intraseasonal (30–60 day) fluctuations of outgoing longwave radiation and 250 mb streamfunction during northern winter. *Mon. Wea. Rev.,* **113,** 941–961.

——, S. J. S. Khalsa, and J. Eischeid, 1992: The atmospheric angular-momentum cycle during the tropical Madden–Julian oscillation. *Mon. Wea. Rev.,* **120,** 2252–2263.

——, G. Kiladis, and P. Sardeshmukh, 1997: The dynamics of intraseasonal atmospheric angular momentum oscillations. *J. Atmos. Sci.,* **54,** 1445–1461.

Welch, B. L., 1947: The generalization of ''Student's'' problem when several different population variances are involved. *Biometrika,* **34,** 28–35.

Wheeler, M. C., and H. H. Hendon, 2004: An all-season real-time multivariate MJO Index: Development of an index for monitoring and prediction. *Mon. Wea. Rev.,* **132,** 1917–1932.

Yanai, M., and M. M. Lu, 1983: Equatorially trapped waves at the 200-mb level and their association with meridional convergence of wave energy flux. *J. Atmos. Sci.,* **40,** 2785–2803.

Yang, G. Y., and B. J. Hoskins, 1996: Propagation of Rossby waves of nonzero frequency. *J. Atmos. Sci.,* **53,** 2365–2378.

Zhang, C., and P. J. Webster, 1992: Laterally forced equatorial perturbations in a linear model. Part I: Stationary transient forcing. *J. Atmos. Sci.,* **49,** 585–607.

——, and S. M. Hagos, 2009: Bimodal structure and variability of large-scale diabatic heating in the tropics. *J. Atmos. Sci.,* **66,** 3621–3640.